Available online at www.sciencedirect.com
SCIENCE DIRECT®
Carbon 43 (2005) 219–227
CARBON
www.elsevier.com/locate/carbon

Synthesis and Raman characterization of boron-doped single-walled carbon nanotubes

K. McGuire [a,1], N. Gothard [a], P.L. Gai [b], M.S. Dresselhaus [c], G. Sumanasekera [d], A.M. Rao [a,*]

[a] Department of Physics and Astronomy, Clemson University, Clemson, SC 29634-0978, USA
[b] DuPont, Central Research and Development Laboratories, Experimental Station, Willmington, DE 19880-0356, USA
[c] Department of Physics and Department of Electrical Engineering and Computer Science, Massachusetts Institute of Technology, Cambridge, MA 02139-4307, USA
[d] Department of Physics, University of Louisville, Louisville, KY 40292, USA

Received 28 October 2004; accepted 1 November 2004

Abstract

A systematic study was carried out to dope single-walled carbon nanotube (SWNT) bundles with varying amounts of boron using the pulsed laser vaporization technique. Targets containing boron concentrations ranging from 0.5 to 10 at.% boron were prepared by mixing elemental boron with carbon paste and the Co/Ni catalysts. The laser-generated products that were obtained from these targets were characterized by high resolution transmission electron microscopy, electron energy loss spectroscopy (EELS), thermoelectric power (TEP) measurements, and Raman scattering experiments. Electron microscopy and Raman studies revealed that the presence of various levels of boron concentration in the target strongly affected the products that were prepared. SWNTs were found in the products prepared from targets containing up through 3 at.% boron, and high resolution EELS estimated that less than 0.05–0.1 at.% boron is present in the SWNT lattice. The absence of SWNT bundles in the products derived from targets containing more than 3 at.% boron implies that the presence of excess boron in the carbon plume severely inhibits the carbon nanotube growth. The overall effect of the boron incorporation primarily leads to: (i) a systematic increase in intensity of the disorder-induced band (D-band) upon boron doping, with increasing D-band intensity observed for higher doping levels, (ii) a systematic downshift in the G′-band frequency due the relatively weaker C–B bond, and (iii) a non-linear variation in the RBM and G′-band intensities which is attributed to shifts in resonance conditions in the doped tubes. Resonant Raman spectroscopy thus provides large changes in the intensity of prominent features even when the dopant concentration is below the detectable limit of EELS (0.05–0.1 at.%). Thermoelectric power data also provide complementary evidence for the presence of a small boron concentration in the SWNT lattice which transforms the SWNTs into a permanently p-type material.

Keywords: A. Carbon nanotubes; B. Doping; C. Electron energy loss spectroscopy, Raman spectroscopy; D. Electrical (electronic) properties

1. Introduction

The possibility of substitutional doping in carbon nanotubes with boron or nitrogen has generated intense interest due to the feasibility of tailoring structural and electronic properties of carbon nanotubes by using boron and nitrogen dopants [1–7]. Doped nanotubes offer the opportunity to not only help in understanding dopant-induced perturbations on physical properties in one-dimensional materials, but such doping also provides an opportunity to exploit their unique properties in the next generation technologies.

* Corresponding author.
E-mail address: arao@clemson.edu (A.M. Rao).
[1] Present address: Department of Physics, University of North Carolina, Chapel Hill, NC 27599, USA.

0008-6223/$ - see front matter © 2004 Published by Elsevier Ltd.
doi:10.1016/j.carbon.2004.11.001

Boron doping in carbon-based materials has been studied for quite some time starting with boron-doped graphite [8–14] to boron-doped carbon nanotubes [15–20]. Straightforward synthesis methods developed for boron-doped graphite have been used to prepare boron-doped single wall carbon nanotube (SWNT) bundles which usually involve heating as-prepared SWNT bundles at high temperatures (1523–1803 °C) with boron-containing compounds, such as B_2O_3 [17]. However, studies aimed at controlled doping and characterization of boron-doped SWNT bundles is lacking.

Based on research reported in boron-doped graphite, novel structural and vibrational properties are anticipated in boron-doped SWNTs, since carbon nanotubes can be viewed as rolling up graphene sheets into seamless cylinders with diameters in the range 1–2 nm. X-ray diffraction studies on boron-doped graphite found that the effect of boron substitution in the hexagonal lattice of graphite led to an increase in the in-plane spacing a and a decrease in the inter-planar spacing c [8]. More recent studies, employing scanning tunneling and atomic force microscopy have confirmed these boron-induced changes in the graphite lattice parameters [9,11]. Interestingly, it was found that the effect of the boron dopant was highly localized with regard to both the structural and electronic properties of graphite, approximately extending up to the next-nearest neighboring carbon atoms in the lattice. Raman studies in boron-doped graphite have shown that the modes most affected by the boron substitution are the disorder-induced D-band at ~1300–1360 cm^{-1} and the G′-band at ~2600–2720 cm^{-1} [9,10]. The D-band intensity increased systematically as the boron concentration reached 2.2 at.% and downshifted by ~3 cm^{-1} [9,10]. A small upshift of the G-band at 1581 cm^{-1} by ~6 cm^{-1} has also been reported when boron concentration exceeded 2 at.% [9,10]. Other carbon materials that have been doped with boron include carbon fibers and multi-walled carbon nanotubes (MWNTs) [18–20]. In these sp^2 carbon materials, the Raman spectra show results similar to those observed in boron-doped graphite.

In this paper, we describe the preparation of a boron and metal catalyst impregnated carbon target which allowed us to prepare SWNT bundles with nominal target boron concentrations from 0.5 to 10 at.% boron using a pulsed laser vaporization process. The novelty of our approach lies in the in situ doping of SWNTs. High resolution transmission electron microscopy (HRTEM), thermopower (TEP), and Raman scattering studies, employing three different laser excitation energies, were used to elucidate the structural and vibrational properties of semiconducting and metallic SWNT bundles prepared from 5 targets, each containing a different boron concentration in the range 0.5–10 at.% boron. In this way, the effect of boron concentration in the target on the structure and properties of the products could be studied systematically. The results showed that the products were strongly affected by the boron concentration present in the targets, and that the nanotube constituent of the sample itself was sensitively affected by boron addition as evidenced through resonant Raman scattering and TEP measurements. Compared to high resolution EELS, the Raman and TEP measurements were found to be much more sensitive to boron addition.

2. Experimental

Single-walled carbon nanotube samples used in this study were prepared by the laser vaporization method. Briefly, a target is placed in a quartz tube and heated to ~1100 °C in an argon atmosphere at a pressure of ~500 Torr. A gentle flow of argon is maintained throughout the process. A Nd:YAG laser (1064 nm, 10 Hz) is then used to ablate the target. Five targets were made using a carbon paste mixed with cobalt:nickel catalyst (0.5:0.5 at.%) and elemental boron. Each boron-doped target had a different nominal at.% boron concentration in the range 0.5–10 at.%. An undoped target (0 at.% boron) was also prepared as a standard for comparison in this systematic study. The SWNTs, when present in the products, had a diameter distribution of 1.3 nm ± 0.2 nm. The carbon paste containing an appropriate catalyst/boron mix was heated to ~200 °C in air, while simultaneously the target was held under a pressure of ~2 metric tons. The targets were then annealed at 1000 °C under flowing argon for ~4 h.

To characterize the SWNT samples used for the Raman and thermopower studies, HRTEM studies were done on the samples prepared from pristine and boron-doped targets, using a novel Tecnai high resolution HR(S)TEM equipped with a 200 kV field emission gun (FEG) [21]. The objective lens spherical aberration coefficient (C_s) is 0.5 mm and the electron wavelength (λ) = 0.0025 nanometers (nm) for the HR(S)TEM instrument. A double-tilt sample stage is used in the HRTEM which provides tilting of crystals in the sample to +24° or −24° and the objective lens of the electron microscope serves as a Fourier transformer. The electron diffraction pattern formed at the back focal plane of the lens is further Fourier transformed to provide the image. Electron waves undergo phase changes during interactions with the sample. The availability of charge coupled device (CCD) cameras has enabled the digital recording of images. For characterization of the boron-doped samples, we combined atomic resolution imaging with high precision chemical and electron nano-diffraction analyses as well as nano-electron energy loss spectroscopy (EELS). Details of the structural properties of the samples used in the present study are reported elsewhere [21].

The thermoelectric power (TEP) was measured, using two Chromel/Alumel thermocouples and two additional Cu leads (all 0.003″ dia. bare wires) that were attached to the edges of the sample which was pressed into a pellet (~5 mm dia; ~1 mm thick) with small amounts of silver epoxy [22]. The TEP data were collected using a heat pulse technique described previously [23,24].

Raman scattering studies were carried out using three different laser excitation wavelengths—514.5, 647.1 and 1064 nm in two spectrometers, namely a JY-Horiba TRIAX 550 single grating spectrometer with a liquid nitrogen cooled CCD detector and a Bruker FT-Raman spectrometer equipped with a liquid nitrogen cooled Ge detector. The TRIAX spectrometer slit width was set to 0.2 mm and the groove density of the grating is 1200 grooves/mm. The spectral resolution in both spectrometers was found to be ~2 cm^{-1}. Argon ion (514.5 nm), krypton (647.1 nm) and Nd: YAG (1064 nm) lasers were used as excitation sources. The excitation beam was brought to a strip or spot focus onto the samples at a power level of 10–20 mW with data being collected in a back scattering geometry. All data were collected from samples maintained at room temperature under ambient conditions.

3. Results and discussion

3.1. High resolution TEM and EELS

Fig. 1 shows the HRTEM images of carbon products obtained after ablating undoped (a), 2.5 at.% (b), and 10.0 at.% (c) boron-doped carbon targets. Henceforth, the boron doping concentrations in the samples (whose results are described below) are expressed in terms of the nominal boron content present in the corresponding target. It can be seen from these images that SWNT bundles are abundant in the products derived from the low boron content (<3 at.%) target material (Fig. 1b). Products resulting from the ablation of a target with boron content >3.5 at.% contain predominantly graphite encapsulated boron carbide particles (Fig. 1c) and a much smaller number of SWNT bundles. Interestingly, a small fraction of the products prepared from a nominal 4.5 at.% boron-doped target contained double walled nanotubes [21]. This decline in nanotube yield with increasing boron content in the target is strongly correlated with the saturation limit of ~3 at. % for boron substitution in the graphite lattice [8,13]. In the products generated using the highly doped targets (>nominal

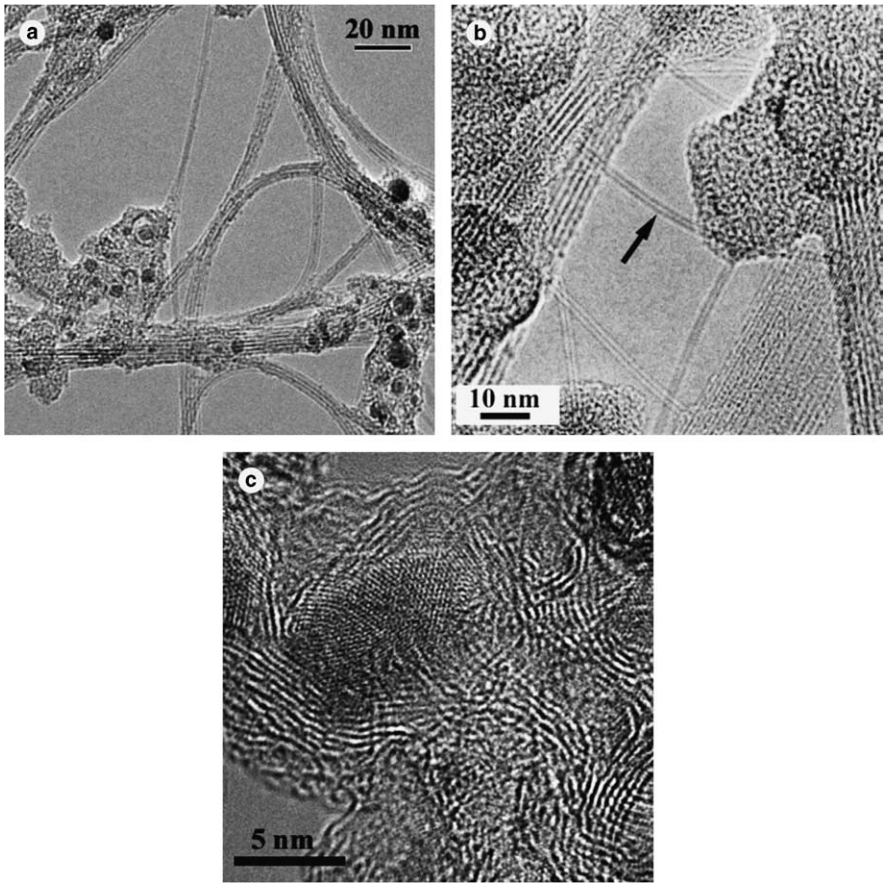

Fig. 1. TEM images of the carbonaceous material produced from targets with nominal boron concentrations of (a) 0 at.%, (b) 2.5 at.%, and (c) 10 at.% boron. SWNTs are clearly present in the material generated from the undoped and 2.5 at.% boron-doped targets.

3 at.% boron), the Co/Ni catalyst particles are found to be saturated by boron, which was interpreted to indicate that the presence of boron in the catalyst particles suppresses SWNT growth [21]. Using in situ diagnostic spectroscopy, Lange et al. concluded in their study involving boron-doped fullerenes that the increased presence of boron (>nominal 3 at.%) in the growth environment can inhibit the formation of C_2 radicals in the plasma region during growth [25]. These observations are consistent with the low SWNT content in products obtained from the highly boron-doped targets used in this study. Nano-EELS measurements failed to detect any boron substituted in the nanotube lattice in any of the samples prepared from the boron enriched target materials in the present study [21]. However, the detection limit of the nano-EELS instrument is ~0.05–0.1 at.% boron. Thus, if any boron is indeed substituted in the SWNT lattice, it is below this limit. We therefore used TEP and Raman measurements to look for the effect of a low concentration of boron on the electronic and vibrational properties of SWNT bundles.

3.2. Thermopower measurements

It has been experimentally shown that semiconducting carbon nanotubes can work as efficient field-effect transistors (CNTFETs) [26–28]. However, the performance characteristics of these CNTFETs when compared to those of analogous silicon devices are inferior from the standpoint of long term device operation. The current–voltage (I–V) characteristics of air-exposed CNTFETs resemble that of a p-type device. Upon annealing under vacuum, the CNTFETs exhibit n-type characteristics. Interestingly, this unexpected transformation from to p- to n-type characteristics is fully reversible, i.e., re-exposure to oxygen brings back the p-type characteristics of the CNTFET. A similar trend was also observed in the temperature-dependent thermopower (TEP) measurements of SWNT bundles and multi-walled carbon nanotube (MWNT) films [24,29,32]. The annealed MWNT film exhibits negative TEP values implying n-type characteristics, which turns to positive TEP values as the sample ages under ambient conditions of room light and room air. Research by several groups proved that the p-character of the CNTFET (or the positive TEP) is not an intrinsic property of the nanotubes and results solely from the interaction of oxygen with the nanotube or from the Schottky barriers at the metal electrode/nanotube contacts. To enable nanotubes to function as a basic building block in future nanoelectronic devices, it is crucial that the oxygen-induced reversal of electronic properties be arrested. One approach is to dope nanotubes with either nitrogen or boron to render them permanently with n-type or p-type characteristics, respectively.

In Fig. 2 we compare the thermopower data obtained from purified-pristine SWNTs (crosses) with those of as-prepared SWNTs generated from the nominal 1.5 at.% boron-doped target (open circles). The TEP data of both samples were collected as a function of time as they were degassed in 10^{-6} Torr vacuum at 500 K. It is clearly seen that, as adsorbed oxygen is removed from the pristine SWNT sample, the thermopower changes sign from approximately +20 μV/K (p-type) to −20 μV/K (n-type), which is expected and similar results have been reported in previous publications [30–32]. Contributions from other impurities present in the as-prepared nanotubes do not affect the TEP sign reversal [30–32]. The sign of the TEP can be used to determine the charge of the dominant carriers in the SWNTs. If the TEP is positive (negative), then the charge carriers are primarily holes (electrons). In the case of the SWNT samples derived from the as-prepared nominal 1.5 at.% boron-doped targets, the TEP remains constant at ~60 μV/K, implying a greater stability of the doped nanotubes with respect to the degassing procedure. This result seems to suggest that a small percentage of the boron is present in the SWNT lattice in concentrations below the detection limit of the electron microscope studies, which is ~0.05–0.1 at.% boron. Substituted boron would be expected to donate holes to the SWNT lattice making it a permanently p-type material, resulting in no change in the TEP as the sample is degassed. The low concentration level of boron in the SWNT lattice is an interesting result since the saturation limit of boron in graphite can be as high as 3 at.% [8]. These results indicate that the solubility of boron in the SWNT lattice is much lower than in planar graphite, possibly due to curvature effects of the nanotubes.

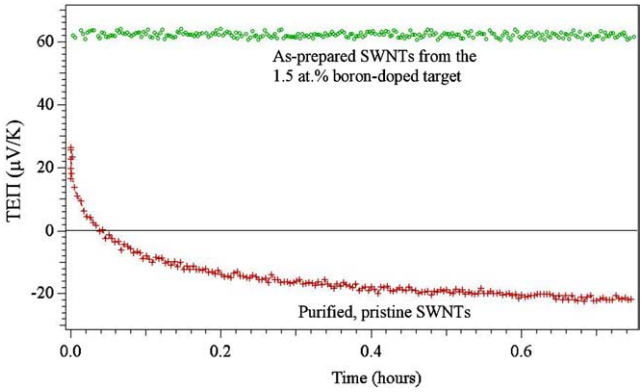

Fig. 2. Comparison of the thermopower data for the purified, pristine SWNT material and the SWNTs produced from the nominal 1.5 at.% boron-doped target. In both data sets the sample was held at 500 K and 10^{-6} Torr vacuum.

It has been shown experimentally and theoretically that boron doping in nanotubes gives rise to a prominent acceptor band near the Fermi level, and as a result, the nanotubes are rich in holes [33]. Therefore, as the hole concentration is depleted during the degassing step, the presence of the acceptor band ensures that the boron-

doped tubes exhibit permanent p-type character. Finally, it should be mentioned that pressed pellets could not be prepared for TEP measurements using products generated from higher boron-containing targets, due to the brittleness of the material grown from targets where the boron content was greater than a nominal 3.5 at.%.

3.3. Raman scattering

Raman scattering has been shown to serve as an excellent probe for investigating the electronic and phonon structure in pristine and doped SWNT materials due to the resonant coupling of the laser excitation energy to the transition energies between the van Hove singularities (vHSs) in the electronic density of states (DOS) [34–39]. Since the energies of the vHSs in the DOS differ from tube to tube based on the tube diameter and chiral angle, specific (n,m) tubes can be studied using this technique. Fig. 3 shows a Kataura plot ($\gamma_0 = 2.90$ eV), which is a plot of vHSs transitions energies vs. the tube diameter [40]. This plot has been very useful in predicting whether semiconducting (crosses) or metallic SWNTs (open circles) will be seen in the Raman spectra for a given laser excitation wavelength. The notation, E^{y}_{xx}, is used to identify a particular transition energy ($x = 1,2,3,\ldots$) in a semiconducting ($y = \mathrm{S}$) or metallic ($y = \mathrm{M}$) SWNT. The two dashed vertical lines in Fig. 3 give the variance σ from the center of a Gaussian distribution of tube diameters around the mean diameter (1.3 ± 0.2 nm) while the horizontal lines indicate the laser energies (2.41, 1.96, and 1.17 eV) used for exciting the Raman spectra (514.5 nm, 647.1 nm, and 1064 nm). Using the known diameter distribution of the sample and the excitation energies of the sources, it is illustrated (Fig. 3) that the 514.5 nm/1064 nm and the 647.1 nm laser excitations will couple resonantly with semiconducting and metallic SWNTs, respectively.

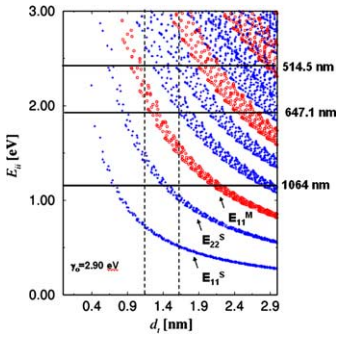

Fig. 3. A Kataura plot of the interband transition energies E_{ii} vs. nanotube diameter in which the range between the two dashed vertical lines represent the SWNT diameter distribution (1.3 ± 0.2 nm) investigated in this study. The horizontal lines help identify the particular E^{y}_{xx} energy transitions to which the 514.5, 647.1 and 1064 nm excitations couple resonantly. See text for definition of E^{y}_{xx}.

In Fig. 4, room temperature Raman spectra for semiconducting SWNTs excited with 514.5 nm excitation are shown. Fig. 4a focuses on the spectral region from 100–1850 cm^{-1}, which contains the first-order features of the SWNT Raman spectrum, while Fig. 4b depicts the second-order Raman spectra for the same set of samples. For products derived from targets with boron concentration $\leqslant$ nominal 3 at.%, the presence of the radial breathing mode (RBM) in their Raman spectra (Fig. 4a) signifies the presence of SWNT bundles in the sample, consistent with the HRTEM study described above (see Fig. 1). Based on a Lorentzian line fit to the data, the RBM at $\sim$186 cm^{-1} and the tangential mode (G-band) at $\sim$1590 cm^{-1} do not show significant shifts or line broadening due to the low boron doping. This is a clear indication that the nanotube structure, as a whole, remains intact in products obtained from targets containing up to nominal 3 at.% boron, which is consistent with the results of the TEM study [21]. However, the disorder-induced D-band at $\sim$1340 cm^{-1} does show a systematic increase in intensity which suggests that the increasing presence of boron in the target is, in fact, bringing about a noticeable change in the degree of ordering in the hexagonal lattice. This increase in the D-band intensity is attributed to the activation of off-zone-center phonons due to relaxation of the strict selection rules for Raman scattering due to a double resonance process [33]. The increasing intensity of the D-band is not surprising, since it is well known that boron doping in highly oriented graphite (HOPG) films leads to increased disorder in the hexagonal lattice as reported by Hishiyama et al. [10] Graphite films with 0.4 and 2.2 at.% boron were examined in their study using the 514.5 nm excitation wavelength [10]. In the 0.4 at.% boron-doped films, the D- and G′-band frequencies softened by $\sim$5 cm^{-1} while the G-band frequency remained pinned at $\sim$1585 cm^{-1} [10]. When the boron concentration further increased from 0.4 at.% and reached 2.2 at.%, the D-band frequency upshifted by $\sim$2 cm^{-1} while the G-band frequency upshifted by $\sim$6 cm^{-1} and the G′-band further softened by 12 cm^{-1}. The net result was an overall downshift of 3 and 17 cm^{-1} respectively, for D and G′-band frequencies, and an upshift of 6 cm^{-1} for the G-band frequency as the boron concentration increased from 0 to 2.2 at.% [10]. It is interesting to note that the G′-band frequency was most sensitive to the boron concentration present in their films. Further, the Hall coefficient measured at 3 K for each of their boron-doped films was positive, implying the presence of holes in the sample, which results in an upshift in the G-band frequency for boron concentration exceeding $\sim$2 at.%. This upshift in the G-band frequency is not expected in the samples used in this study, since nano-EELS measurements indicated that the presence of boron in SWNT bundles obtained from ablating 3 at.% boron-doped targets was less than 0.05–0.1 at.%. It

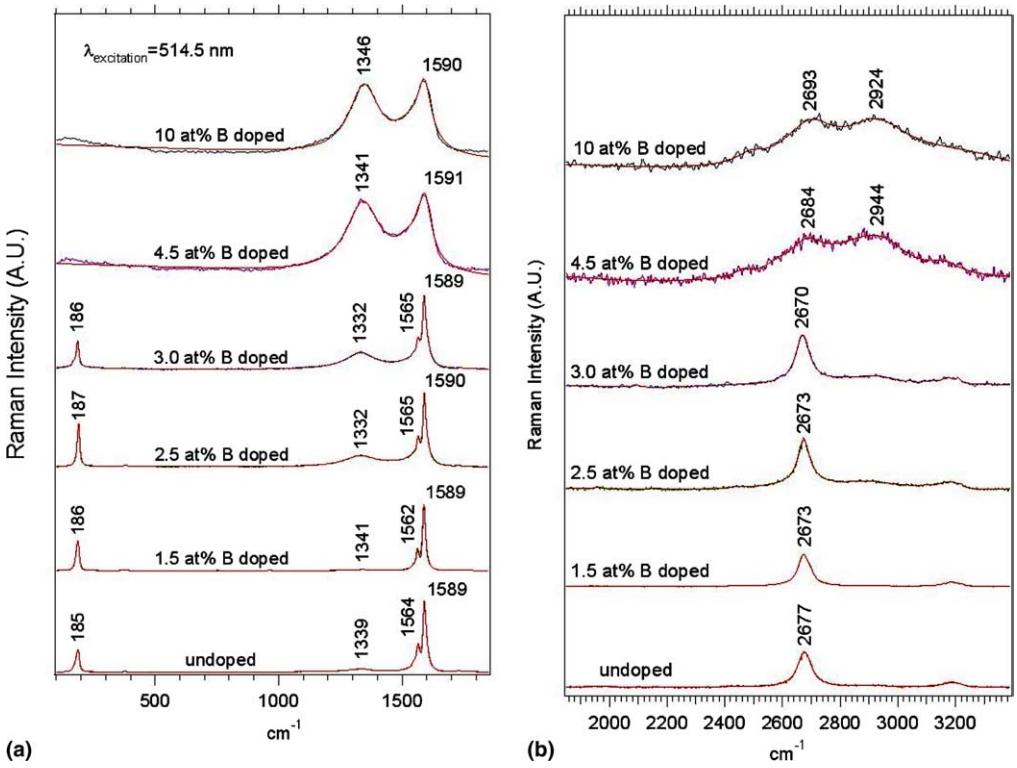

Fig. 4. (a) First-order and (b) second-order room temperature Raman spectra of products generated from targets with indicated boron concentrations. All Raman spectra were excited using the 514.5 nm excitation energy. Each spectrum in the figure was normalized to the tangential G^+ band intensity.

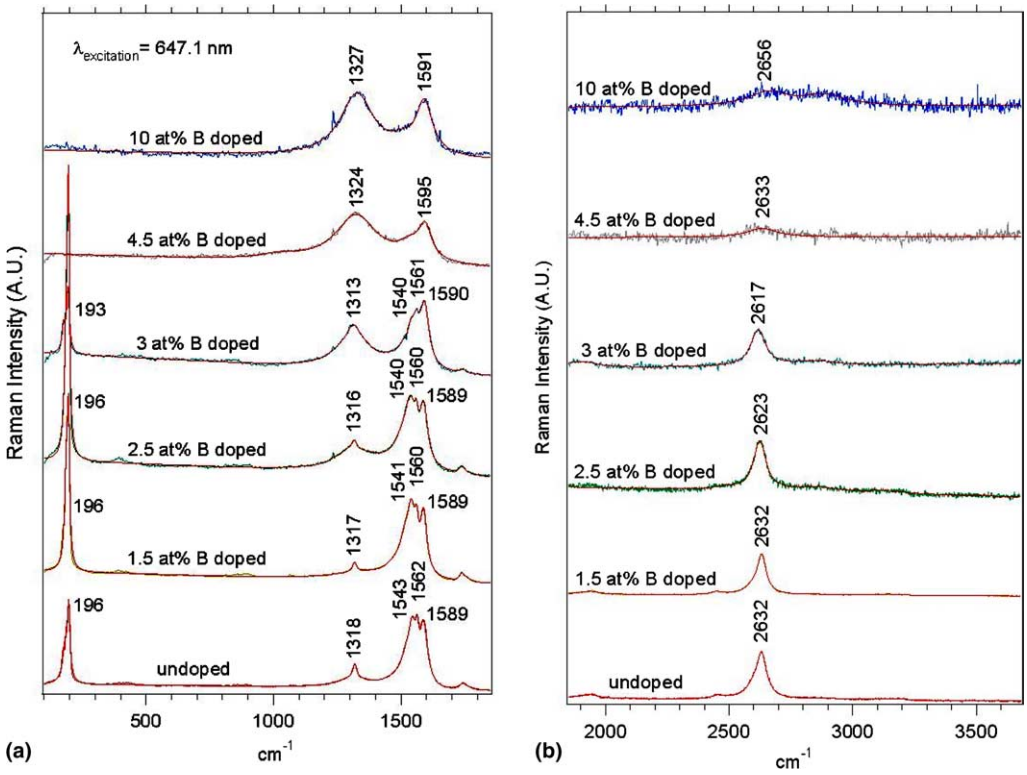

Fig. 5. (a) First-order and (b) second-order room temperature Raman spectra of products generated from targets with indicated boron concentrations. All Raman spectra were excited using the 647.1 nm excitation energy. Each spectrum in the figure was normalized to the tangential G^+ band intensity.

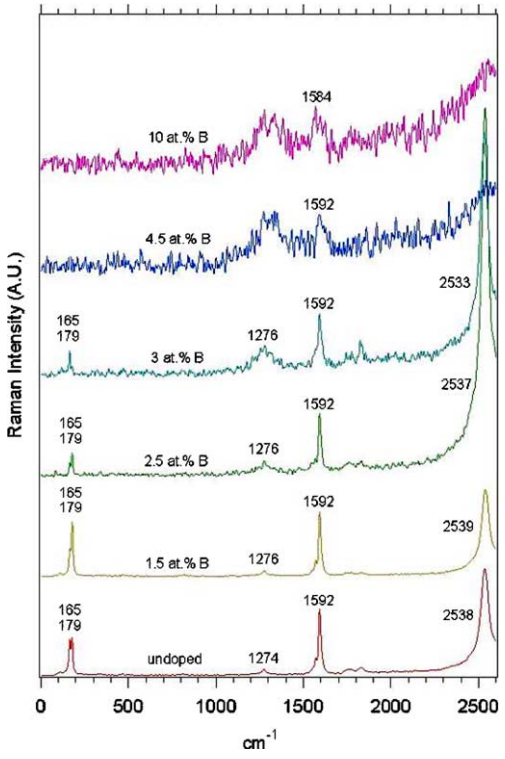

Fig. 6. First-order and second-order room temperature Raman spectra of products generated from targets with indicated boron concentrations. All Raman spectra were excited using the 1064 nm excitation energy. Each spectrum in the figure was normalized to the tangential G^+ band intensity.

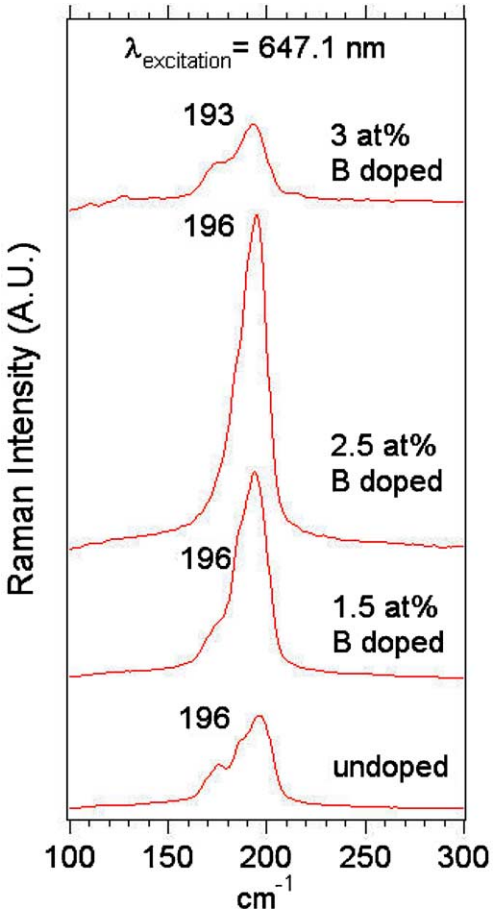

Fig. 7. Expanded plot of the RBM intensity enhancements (discussed in Fig. 5a) plotted as a function of the boron concentration present in the target. The data were collected using the 1.96 eV excitation energy (647.1 nm).

should be noted that, consistent with the work of Hishiyama et al., the G-band frequency at 1591 cm^{-1} can be seen in the Raman spectrum of the products generated from the 10 at.% boron target which did not contain nanotubes. Also, the D-band frequency is downshifted by ~7 cm^{-1} as the boron concentration in the target was increased from 0 to 3 at.% (Fig. 4a).

The disappearance of the RBM and the accompanying broadening of the G- and D-bands in the Raman spectrum observed at three different excitation wavelengths (Figs. 4–6) of products produced from targets with boron concentrations above the nominal 3 at.% signifies that no SWNTs are formed. In other words, the Raman spectra for samples from targets with more than the nominal 3 at.% boron resemble that of disordered sp^2 carbon materials. Interestingly, this finding strongly correlates with the maximum boron solubility of ~3 at.% that is known in the graphite literature [8]. In addition, the HRTEM/nano-EELS studies show that in samples grown from targets containing more than the nominal 3 at.% boron, the increased boron concentration present in the catalyst particles diminishes the efficiency of these particles for catalyzing the growth of SWNTs [21]. However, Fig. 4b shows that the G′-band at 2677 cm^{-1} in the pristine SWNT bundles systematically downshifts with increasing B concentrations, reaching a value of 2670 cm^{-1} in the nominal 3 at.% boron-doped sample, without a detectable increase in its linewidth. Revisiting the study of Hishiyama et al., the G′-band *downshifts* from 2725 cm^{-1} in a HOPG film to 2720 cm^{-1} in 0.4 at.% boron-doped HOPG film [10]. This band further downshift to 2708 cm^{-1} in the 2.2 at.% boron-doped film. The G′-band *downshifts* presumably as a result of the weaker C–B bond compared to the C–C bond energies.

It is known that the G′-band exhibits a chirality and diameter dependence based on previously reported work on hole doped SWNTs [39]. However, one observation that can be made suggests that this is not the cause of the shift in the G′ peak position in Fig. 4b. The RBM frequency remains the same for all boron-doping levels (Fig. 4a) and this observation is consistent with a highly localized acceptor band observed in STS studies of boron-doped MWNTs [33].

Raman data were also collected from metallic SWNTs in the sample using the 647.1 nm (1.96 eV) laser excitation. The results are presented in Fig. 5 in the same fashion as for the semiconducting tubes in the boron-doped

SWNT bundles. In these spectra, similar trends are also observed in the frequencies of the RBM, G-, D-, and G′-modes with the exception that the G′-band is downshifted in frequency to a greater extent (by $\sim 15\,cm^{-1}$) in SWNTs grown from the nominal 3 at.% boron-doped target.

Motivated by this observation of a greater downshift in the G′-band frequency for metallic SWNTs, we examined the Raman spectra of the same set of samples using the 1064 nm laser excitation (Fig. 6). The results in Fig. 6 show Raman spectra for semiconducting tubes with the radial breathing modes appearing at 165 and $179\,cm^{-1}$. Again, similar trends are seen in these spectra (lack of significant frequency shifts for the RBM and G-band, an increased D-band intensity, and a $\sim 5\,cm^{-1}$ downshift of G′-band position) with the exception that the D-band frequency is found slightly upshifted by $\sim 2\,cm^{-1}$.

The huge intensity for the G′-band in Fig. 6 is certainly noteworthy, and is attributed to boron-induced changes in the electronic properties of SWNTs as is discussed next. A more careful examination of the spectra in Figs. 4a and 5a shows that the intensities of the RBM vary non-linearly with the at.% boron present in the target. For example, the intensity for the RBM in Fig. 4a is largest when the boron concentration in the target reaches 2.5 at.%. Likewise, the intensity for the RBM in Fig. 5a is also largest at 2.5 at.% boron concentration as depicted in Fig. 7 for clarity. These observations are attributed to a shift in the resonance conditions induced by the presence of boron in the SWNT lattice which shifts the E_{xx} by a few meV, thereby bringing nanotubes further into resonance with the incident or scattered photon. A detailed scanning tunneling spectroscopy/microscopy (STM/STS) study is needed to fully understand these resonance effects. Tentatively, we conclude that the resonance is achieved for laser excitation energy of $E_{laser} = 1.17\,eV$ (1064 nm) with the scattered photon, since changes in the G′-band intensity with the boron doping of the target material is dominant over the changes in the RBM intensities (Fig. 6). In contrast, for excitation energies at 1.96 eV (647.1 nm) and 2.41 eV (514.5 nm), we conclude that resonance is achieved with the incident photon, since the dominant changes are observed for intensities associated with the RBM.

4. Conclusions

The data from the high resolution EELS, thermoelectric power measurements, and Raman scattering experiments, when considered together, suggest the presence of small concentrations of boron in the SWNT lattice and that this boron concentration is extremely small compared to the amount of boron introduced into the synthesis environment. The SWNT growth ceases when a large amount of boron (>nominal 3 at.% boron) is present in the starting target material. This reduction in SWNT growth may be due to the poisoning of the catalyst particle which seeds the growth of the nanotubes. While no clear evidence for boron is seen in the SWNT lattice using electron microscopy measurements (within the instrument detection limit of 0.05–0.1 at.% boron), the sign reversal of the TEP and large changes in the Raman spectra do indicate that changes to the electronic and structural properties of the sample are taking place due to the presence of boron. The amount of boron in the nanotubes is estimated to be below the electron microscope detection limit. The results of the Raman scattering experiments show that the effect of the boron in the synthesis of SWNTs primarily causes: (i) a systematic increase in the D-band intensity, (ii) a systematic softening of the G′-band without significant changes in the RBM and G-band frequencies, (iii) changes in the electronic properties of doped SWNT bundles as evidenced by intensity enhancement in the RBM observed at laser excitation wavelengths for the incident photon (Figs. 4a, 5a, 7), and (iv) large changes in the G′-band intensities at 1064 nm excitation associated with the scattered photon (Fig. 6).

Acknowledgments

The research at Clemson University was supported in part by NSF grants numbers: 0304019, 0244290 and 0216307. MSD gratefully acknowledges support from the DuPont MIT alliance for the MIT contribution to this research project.

References

[1] Ouyang M, Huang JL, Lieber CM. Annu Rev Phys Chem 2002;53:201–20.
[2] Rochefort A, Salahub DR, Avouris P. Chem Phys Lett 1998;297:45–50.
[3] Fuhrer MS, Cohen ML, Zettl A, Crespi V. Solid State Commun 1999;109:105–9.
[4] Avouris P, Hertel T, Martel R, Schmidt T, Shea HR, Walkup RE. Appl Surf Sci 1999;141:201–9.
[5] Appenzeller J, Martel R, Derycke V, Radosavljević V, Wind S, Neumayer D, et al. Microelectron Eng 2002;64:391–7.
[6] Bachtold A, Hadley P, Nakanishi T, Dekker C. Physica E 2003;16:42–6.
[7] Terrones M, Jorio A, Endo M, Rao AM, Kim YA, Hayashi T, et al. Mater Today Mag 2004(October):30–45.
[8] Lowell CE. J Amer Ceram Soc 1967;50:142.
[9] Endo M, Hayashi T, Hong S-H, Enoki T, Dresselhaus MS. J Appl Phys 2001;90:5670–4.
[10] Hishiyama Y, Irumano H, Kaburagi Y, Soneda Y. Phys Rev B 2001;63:245406-1–11.
[11] Kim E, Oh I, Kwak J. Electochem Commun 2001;3:608–12.
[12] Ma X, Wang Q, Chen L-Q, Cermignani W, Schobert HH, Pantano CG. Carbon 1997;35:1517–25.
[13] Serin V, Brydson R, Scott A, Kihn Y, Abidate O, Maquin B, et al. Carbon 2000;38:547–54.

[14] Hagio T, Nakamizo M, Kobayashi K. Carbon 1989;27:259–63.
[15] Czerw R, Chiu PW, Choi YM, Lee DS, Carroll DL, Roth S, et al. Curr Appl Phys 2002;2:473–7.
[16] Redlich P, Loeffler J, Ajayan PM, Bill J, Aldinger F, Rühle M. Chem Phys Lett 1996;260:465–70.
[17] Golberg D, Bando Y, Han W, Kurashima K, Sato T. Chem Phys Lett 1999;308:337–42.
[18] Endo M, Kim C, Karaki T, Tamaki T, Nishimura Y, Matthews MJ, et al. Phys Rev B 1998;58:8991–6.
[19] Liu K, Avouris P, Martel R, Hsu WK. Phys Rev B 2001;63:161404–7.
[20] Hsu WK, Nakajima T. Carbon 2002;40:462–5.
[21] Gai PL, Stephan O, McGuire K, Rao AM, Dresselhaus MS, Dresselhaus G, et al. J Mater Chem 2004;14:669–75.
[22] Sumanasekera GU, Grigorian L, Eklund PC. Meas Sci Technol 2000;11:273–7.
[23] Eklund PC, Mubatah AK. Rev Sci Instr 1977;48:775–7.
[24] Sumanasekera GU, Adu CKW, Fang S, Eklund PC. Phys Rev Lett 2000;85:1096–9.
[25] Lange H, Huczko A, Byszewski P, Mizera E, Shinohara H. Chem Phys Lett 1998;289:174–80.
[26] Tans SJ, Verschueren RM, Dekker C. Nature 1998;393:49–52.
[27] Martel R, Schmidt T, Shea HR, Hertel T, Avouris P. Appl Phys Lett 1998;73:2447–9.
[28] Soh HT, Quate CF, Morpurgo AF, Marcus CM, Kong J, Dai H. Appl Phys Lett 1999;75:627–30.
[29] Savage T, Bhattacharya S, Sadanadan B, Gaillard J, Tritt T, Sun Y-P, et al. 2003;15:5915–21.
[30] Pradhan BK, Harutyunyan AR, Stojkovic D, Grossman JC, Zhang P, Cole MW, et al. Mater Res Soc Symp Proc 2002;706:Z10.3.1–.6.
[31] Adu CKW, Sumanasekera GU, Pradhan BK, Romero HE, Eklund PC. Chem Phys Lett 2001;337:31–6.
[32] Collins PG, Bradley K, Ishigami M, Zettl A. Science 2000;287:1801–4.
[33] Carroll DL, Ajayan PM, Curran S. J Mater Res 1998;13:2389–95.
[34] Rao AM, Richter E, Bandow S, Chase B, Eklund PC, Williams KA, et al. Science 1997;275:187–91.
[35] Dresselhaus MS, Jorio A, Souza Filho AG, Dresselhaus G, Saito R. Physica B: Condens Matter 2002;323:15–20.
[36] Rao AM, Jorio A, Pimenta M, Dantas MSS, Saito R, Dresselhaus G, et al. Phys Rev Lett 2000;84:1820–3.
[37] Jorio A, Dresselhaus G, Dresselhaus MS, Souza M, Dantas MSS, Pimenta MA, et al. Phys Rev Lett 2000;85:2617–21.
[38] Thomsen C, Reich S. Phys Rev Lett 2000;85:5214–8.
[39] Dresselhaus MS, Eklund PC. Adv Phys 2000;49:705–814.
[40] Kataura H, Kumazawa Y, Maniwa Y, Umezu I, Suzuki S, Ohtsuka Y, et al. 1998;103:2555–8.